Journal of Materials Chemistry A

Two-step synthesis of Sillén-Aurivillius type oxychlorides to enhance the photocatalytic activity for visible-light-induced water splitting

Journal:	*Journal of Materials Chemistry A*
Manuscript ID	TA-ART-04-2018-003321.R2
Article Type:	Paper
Date Submitted by the Author:	11-May-2018
Complete List of Authors:	Nakada, Akinobu; Kyoto University, Saeki, Akinori; Osaka University, Department of Applied Chemistry, Graduate School of Engineering Higashi, Masanobu; Kyoto University, Kageyama, Hiroshi; Kyoto University, Department of Energy and Hydrocarbon Chemistry Abe, Ryu; Kyoto University, Graduate School of Engineeing

Journal Name

ARTICLE

Two-step synthesis of Sillén-Aurivillius type oxychlorides to enhance the photocatalytic activity for visible-light-induced water splitting

Received 00th January 20xx,
Accepted 00th January 20xx

DOI: 10.1039/x0xx00000x

www.rsc.org/

Akinobu Nakada,[a] Akinori Saeki,[b] Masanobu Higashi,[a] Hiroshi Kageyama*[a,c] and Ryu Abe*[a,c]

A two-step synthesis *via* polymerized complex method (2PC) was developed to improve the photocatalytic activity of a Sillén-Aurivillius oxychloride Bi_4TaO_8Cl and related oxychlorides for O_2 evolution (*i.e.*, water oxidation) in Z-scheme water splitting under visible light. This method uses the polymerized complex reaction to prepare a precursor oxide (e.g., Bi_3TaO_7), which is subsequently calcined with BiOCl to yield a pure Bi_4TaO_8Cl phase with smaller particle sizes than those *via* conventional single-step solid-state reaction (1SSR). Furthermore, time-resolved microwave conductivity (TRMC) measurements revealed that a Bi_4TaO_8Cl sample prepared by 2PC method at 973 K (2PC_973) achieved more than five times longer-lived charge separation than that by 1SSR at 973 K (1SSR_973), which probably arises from lower numbers of charge-recombination center produced in 2PC synthesis. Thus, synthesized Bi_4TaO_8Cl samples exhibited higher rate of O_2 evolution (*e.g.*, 20 μmol h^{-1} for 2PC_973 vs. 4 μmol h^{-1} for 1SSR_973). Simultaneous water splitting into stoichiometric H_2 and O_2 production was demonstrated by constructing Z-scheme photocatalytic system consisting of 2PC_973, Ru-modified $SrTiO_3$:Rh, and an Fe^{3+}/Fe^{2+} shuttle redox mediator, with the external quantum efficiency of 0.9% at 420 nm, much higher than that using the sample derived from the optimized 1SSR method at 1173 K (0.4%). The 2PC synthesis was successfully expanded to other Sillén-Aurivillius type oxychlorides, Bi_4NbO_8Cl, $Bi_6NbWO_{14}Cl$ and $Sr_2Bi_3Ta_2O_{11}Cl$, all of which exhibited superior water splitting activity compared to those prepared through 1SSR.

Introduction

Photocatalytic splitting of water is an attractive research field for sustainable production of clean hydrogen energy by harvesting abundant sunlight. Development of stable and visible-light-active photocatalyst materials such as particulate semiconductors is indispensable to achieve practically high efficiency in the solar to hydrogen conversion *via* such photocatalytic water splitting because visible region possesses almost half energy in sunlight. Mixed-anion and non-oxide materials such as (oxy)nitrides[1–9] and (oxy)sulfides[10–14] have been developed as potential candidates for visible light-induced water splitting. The valence-band levels of the mixed anions can be substantially controlled by hybridization of O-2p and introduced anion orbitals,[15,16] enabling both visible-light absorption and suitable band potentials for both reduction and oxidation of water. However, they generally suffer from self-oxidative deactivation where photogenerated holes oxidize the introduced anions such as N^{3-} and S^{2-} species during photocatalytic reaction.[11,17–22] Appropriate surface modification such as cocatalyst loading is necessary in most cases to circumvent the oxidative deactivation.[1–3,9–12,20,23] Hence, the number of mixed-anion materials available for stable water splitting systems, *via* both one-step and two-step photoexcitations, so-called Z-scheme, are still limited.

We have recently demonstrated that Sillén-Aurivillius layered perovskite oxyhalides such as Bi_4MO_8X (*M* = Nb, Ta; *X* = Cl, Br)[24,25] have unique band structures that offer great possibility of visible-light-induced water splitting. The VBMs in Bi_4MO_8X consist mainly of O-2p orbitals, instead of Cl-3p or Br-4p, with much more negative potential than those of usual oxides or oxychlorides. These features provide visible-light absorption and high photostability, while maintaining sufficiently negative CBM (−0.4 ~ −0.5 V) for water reduction.[24] Thus, the Bi_4MO_8X materials potentially be a leading candidate as the photocatalyst even for one-step water splitting under visible light, although it has not yet achieved probably due to the low activity of Bi_4MO_8X for water reduction. Meanwhile, we have demonstrated that Bi_4MO_8X can function as stable O_2-evolving photocatalysts under visible-light irradiation, without the use of cocatalyst.[24,26–28] For example, Bi_4NbO_8Cl exhibited visible-light-induced O_2 evolution using an Fe^{3+} electron acceptor with the apparent quantum yield (AQY) of 0.4% at 420-nm monochromatic-light irradiation.[26] Furthermore, Z-scheme water splitting has been achieved using the combination of the

[a] Department of Energy and Hydrocarbon Chemistry, Graduate School of Engineering, Kyoto University, Nishikyo-ku, Kyoto 615-8510, Japan. *E-mail: kage@scl.kyoto-u.ac.jp (H.K.); ryu-abe@scl.kyoto-u.ac.jp (R.A.)
[b] Department of Applied Chemistry, Graduate School of Engineering, Osaka University, 2-1 Yamadaoka, Suita, Osaka 565-0871, Japan.
[c] CREST, Japan Science and Technology Agency (JST), Kawaguchi, Saitama 332-0012, Japan.

Electronic Supplementary Information (ESI) available: [XRD patterns, SEM images and photocatalytic water splitting]. See DOI: 10.1039/x0xx00000x

layered perovskite oxyhalides as an O_2-evolving photocatalyst, Ru-modified $SrTiO_3$ doped with Rh as a H_2-evolving photocatalyst, and Fe^{3+}/Fe^{2+} shuttle redox mediator *via* two-step visible-light excitation.[26,27] However, the photocatalytic activities still remain room for improvement.

In general, photocatalytic activities of the inorganic semiconductor are significantly affected by the synthetic procedures.[23,29–34] Given the fact that the photocatalytic properties of Bi_4MO_8X were previously studied using samples prepared by high temperature solid-state reactions (SSR), optimizing synthetic conditions would be a reasonable next step to improve the activities. In this work, we developed a two-step synthesis of Bi_4TaO_8Cl through polymerized-complex reaction and investigated the effects of synthetic procedures on the photocatalytic activities for water oxidation. In addition, time-resolved microwave conductivity (TRMC) measurements of Bi_4TaO_8Cl were employed to examine charge relaxation processes related to the photocatalytic activity. Finally, Z-schematic water splitting was demonstrated by using Bi_4TaO_8Cl as an O_2-evolving part combined with a H_2-evolving photocatalyst (Ru modified $SrTiO_3$:Rh) and an Fe^{3+}/Fe^{2+} shuttle redox mediator. Other layered oxychlorides of Bi_4NbO_8Cl, $Bi_6NbWO_{14}Cl$, and $Sr_2Bi_3Ta_2O_{11}Cl$ were prepared with the two-step synthesis and their photocatalytic properties were compared.

Experimental

Synthesis

As a precursor to synthesize the target Bi_4TaO_8Cl samples *via* a two-step procedure, a particulate Bi_3TaO_7 sample was initially prepared by a polymerized complex (PC) method as follows; $Bi(NO_3)_3{\cdot}5H_2O$ (9 mmol, Wako Pure Chemicals) and $TaCl_5$ (3 mmol, High Purity Chemicals) were mixed in methanol (20 mL) followed by addition of citric acid (0.13 mol, Wako Pure Chemicals). The mixture was stirred at 423 K to produce a transparent solution. After ethylene glycol (32 mL, Wako Pure Chemicals) was added, the solution was heated at 593 K on a hot stirrer with stirring to accelerate polymerization. The obtained brown gel was further heated at 623 K by using a mantle heater, producing a black solid mass. Finally, particulate Bi_3TaO_7 was obtained by calcining the black solid mass on an Al_2O_3 plate at 773 K for 2 h in air. Another Bi_3TaO_7 precursor was also synthesized by a conventional SSR; a stoichiometric mixture of Bi_2O_3 (Wako Pure Chemicals) and Ta_2O_5 (High Purity Chemicals) was heated at 1073 K for 5 h in air. In order to prepare Bi_4NbO_8Cl, $Bi_6NbWO_{14}Cl$, and $Sr_2Bi_3Ta_2O_{11}Cl$ with two-step procedures, particulates of Bi_3NbO_7, Bi_5NbWO_{13} and $SrBi_2Ta_2O_9$ were synthesized by the above-described PC method, using $NbCl_5$ (High Purity Chemicals), $(NH_4)_{10}W_{12}O_4$ (Wako Pure Chemicals), and $SrCO_3$, respectively, as raw materials.

BiOCl was prepared by a soft-chemical method from $Bi(NO_3)_3{\cdot}5H_2O$ (High Purity Chemicals) and KCl (High Purity Chemicals) and used as a precursor. An aqueous KCl solution (0.5 M, 20 mL) was added into an ethanolic $Bi(NO_3)_3{\cdot}5H_2O$ solution (0.17 M, 60 mL) with stirring. The mixture was subsequently stirred at room temperature for 15 h. The obtained precipitate was centrifuged and washed several times with ethanol and water to give a pure BiOCl. $SrBiO_2Cl$, a precursor for $Sr_2Bi_3Ta_2O_{11}Cl$, was also synthesized by calcination of a mixture of BiOCl (10 mmol) and $SrCO_3$ (10 mmol) at 1073 K for 10 h in air.

Bi_4TaO_8Cl, the main target compound in the present study, was synthesized by SSR of the above Bi_3TaO_7 and BiOCl precursors. The Bi_3TaO_7 precursor (1.0 mmol) was thoroughly mixed with BiOCl (1.05 mmol), pelletized and heated in an evacuated silica tube at various temperatures. In all cases, a 5% excess amount of BiOCl was used to compensate a loss due to volatilization during the thermal treatment.[28] The Bi_4TaO_8Cl samples prepared using the Bi_3TaO_7 precursor *via* PC method will be hereafter denoted as Bi_4TaO_8Cl (2PC_*T*), whereas those with Bi_3TaO_7 precursors *via* SSR as Bi_4TaO_8Cl (2SSR_*T*), where *T* represents the calcination temperature (K) employed. For comparison, we also prepared Bi_4TaO_8Cl samples *via* conventional one-step SSR in vacuum from a mixture of Bi_2O_3 (1.5 mmol, Wako Pure Chemicals), BiOCl (1.05 mmol) and Ta_2O_5 (0.5 mmol, High Purity Chemicals) under varied heating temperatures, denoted hereafter as Bi_4TaO_8Cl (1SSR_*T*). These procedures are summarized in Scheme 1.

Other target compounds, Bi_4NbO_8Cl and $Bi_6NbWO_{14}Cl$ were also synthesized by the above-mentioned 2PC method using Bi_3NbO_7 and Bi_5NbWO_{13}, respectively, as starting materials instead of Bi_3TaO_7. For comparison, both Bi_4NbO_8Cl and $Bi_6NbWO_{14}Cl$ were prepared *via* conventional one-step SSR from corresponding single metal oxides and BiOCl according to literatures.[26,27] As for the two-step synthesis of $Sr_2Bi_3Ta_2O_{11}Cl$, a mixture of $SrBi_2Ta_2O_9$ (1.0 mmol) and $SrBiO_2Cl$ (1.05 mmol) was heated at 1123 K for 15 h in air. For comparison, $Sr_2Bi_3Ta_2O_{11}Cl$ was also synthesized *via* conventional one-step SSR by heating a mixture of $SrCO_3$ (2.0 mmol, Wako Pure Chemicals), Bi_2O_3 (1.0 mmol, Wako Pure Chemicals), BiOCl (1.05 mmol) and Ta_2O_5 (1.0 mmol, High Purity Chemicals) at 1223 K for 35 h in air.

As a H_2-evolving photocatalyst, Rh-doped $SrTiO_3$ ($SrTiO_3$:Rh) was prepared by SSR.[35] A mixture of Rh_2O_3 (0.1 mmol, Wako Pure Chemicals), $SrCO_3$ (10.7 mmol, Wako Pure Chemicals) and TiO_2 (9.8 mmol, Wako Pure Chemicals) was heated at 1073 K for 1 h in air followed by heating at 1273 K for 10 h with an intermediate grinding to obtain $SrTiO_3$:Rh. Ru cocatalyst was loaded by a photodeposition method in methanolic (10 vol%) aqueous dispersion of $SrTiO_3$:Rh containing $RuCl_3$ (0.7 wt% based on metal) with visible-light irradiation ($\lambda > 400$ nm) for 2 h.

Characterization

Powder X-ray diffraction (XRD; X-ray source: Cu K_α), scanning electron microscopy (SEM; NVision 40, Carl Zeiss-SIINT), the Brunauer-Emmett-Teller surface area (BET; BELSORP-mini, BEL Japan), UV-visible diffuse reflectance spectroscopy (V-650, JASCO) and X-ray photoelectron spectroscopy (XPS; JPC-9010MC, JEOL, X-ray source: Mg K_α) were used for characterization of the samples. The binding energy determined

by the XPS measurements was corrected with reference to the C 1s peak of impurity carbon (284.8 eV).

Photocatalytic reaction

Photocatalytic reactions were carried out in a Pyrex reaction vessel connected to a glass closed gas circulation system. For the photocatalytic water oxidation, a suspension of photocatalyst (0.2 g) in 250 mL aqueous $FeCl_3$ solution (5 mM, pH 2.5 adjusted by HCl) was purged with Ar and irradiated at $400 < \lambda < 800$ nm using a Xe lamp (Cermax, 300 W) fitted with a CM-1 cold mirror and a L-42 cut-off filter. The solution pH was adjusted to 2.5 using HCl to avoid precipitation of $Fe(OH)_3$. The evolved gases were analyzed by a gas chromatography (GC-8A, Shimadzu, TCD detector, MS 5A column, Ar carrier) connected to the closed gas circulation system.

Overall water splitting was carried out with the same experimental setting for a reaction suspension of the oxyhalide materials and Ru/$SrTiO_3$:Rh (0.1 g each) in an aqueous $FeCl_3$ solution (1 mM, pH 2.5 adjusted by HCl). For $Sr_2Bi_3Ta_2O_{11}Cl$, UV-vis light ($350 < \lambda < 800$ nm) was irradiated by a Xe lamp (Cermax, 300 W) fitted with a CM-1 cold mirror.

To measure the external quantum efficiency, the similar experimental setting was used with a monochromatic light irradiation (λ = 420 nm) using a Xe lamp (Cermax, 300 W) fitted with a CM-1 cold mirror and a band pass filter. The apparent quantum yield (AQY), equivalent to external quantum yield, of Z-scheme water splitting was determined based on eq. 1.

$$\mathrm{AQY}\ (\%) = 100 \times A \times R/I \quad (1)$$

where A is the number of photons required to generate one molecule of products (*i.e.*, 4 for H_2 and 8 for O_2 evolution), R is the rate of gas generation (mol s^{-1}) and I is the incident photon flux (2.2×10^{-7} einstein s^{-1}).

Time-resolved microwave conductivity (TRMC) measurement

TRMC experiments were conducted with the third harmonic generator (THG; 355 nm) of a Nd:YAG laser (Continuum Inc., Surelite II, 5–8 ns pulse duration, 10 Hz) as the excitation source (4.6×10^{15} photons cm^{-2} $pulse^{-1}$) and X-band microwave (~9.1 GHz) as the probe. The photoconductivity $\Delta\sigma$ was obtained by applying the formula $\Delta P_r/AP_r$, where ΔP_r, A, and P_r are the transient power change of the reflected microwave power, the sensitivity factor, and the reflected microwave power, respectively. The photoconductivity transient $\Delta\sigma$ was converted to the product of the quantum yield (φ) and the sum of charge carrier mobilities $\sum\mu$ (= $\mu_+ + \mu_-$) by the formula $\phi\sum\mu = \Delta\sigma(eI_0F_{\mathrm{light}})^{-1}$, where e and F_{light} are the unit charge of a single electron and a correction (or filling) factor, respectively. The experiments were performed in the air at room temperature (298 K).

RESULTS AND DISCUSSION

Synthesis and characterization of Bi_4TaO_8Cl

Scheme 1 summarizes three different preparation procedures of Bi_4TaO_8Cl samples employed in the present study. As described in the experimental section, a precursor Bi_3TaO_7 was preliminarily prepared by a polymerized-complex (PC) method for the newly developed two-step (2PC) synthesis. Almost pure phase of fluorite-type Bi_3TaO_7 was obtained by the PC reaction followed by calcination at 773 K (Fig. S1). On the contrary, a temperature higher than 1073 K was required to complete the reaction for the formation of pure Bi_3TaO_7 when the conventional solid-state reaction (SSR) was used from a mixture of Bi_2O_3 and Ta_2O_5 particles (Fig. S1). The reduction of required temperature in PC method is certainly due to well dispersion of metal cations in the precursor solution and polymer. Therefore, the PC method can provide pure Bi_3TaO_7 with much smaller particle size compared to those prepared *via* SSR as seen in SEM images (Fig. S2), in which particles of several tens nanometers were aggregated. Each Bi_3TaO_7 precursor was subsequently heated with another precursor BiOCl at various temperatures for synthesizing Bi_4TaO_8Cl.

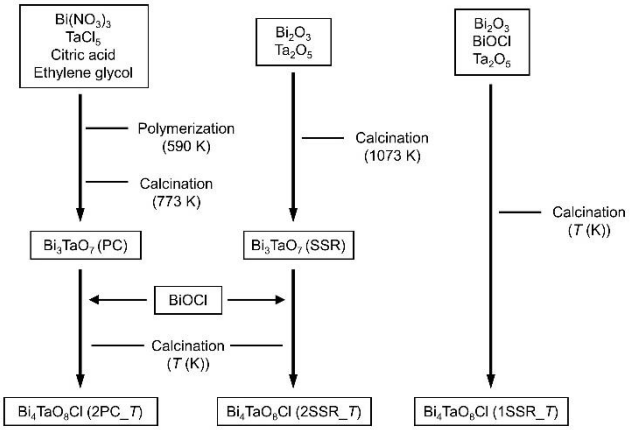

Scheme 1. Synthesis Procedures for Bi_4TaO_8Cl by 2PC, 2SSR and 1SSR Methods.

In the case of 2PC synthesis, a pure phase of Bi_4TaO_8Cl was produced after the reaction with BiOCl at $T \geq 923$ K as confirmed by the XRD patterns (Fig. 1a). On the other hand, reaction at 923 K by 2SSR method gave impurity BiO_x (Fig. 1b), indicating that the use of Bi_3TaO_7 particles prepared by PC method as the precursor is a crucial factor to form a single phase Bi_4TaO_8Cl at lower temperature. Conventional one-step SSR synthesis from Bi_2O_3, BiOCl and Ta_2O_5 at 923 K also gave impurity phases (Fig. 1c). Although the reactions at $T \geq 973$ K always provide a single phase Bi_4TaO_8Cl regardless of the procedures (Fig. 1), the particle size of Bi_4TaO_8Cl produced significantly differs depending on the procedure employed. A comparison between the SEM images of Bi_4TaO_8Cl particles prepared *via* 2PC method and those *via* SSR methods revealed that the 2PC method at any calcination temperature could produce smaller particles (Fig. 2). Especially, the Bi_4TaO_8Cl particles prepared *via* 2PC at 973 K possess smaller particle size ranging from 100 to 300 nm compared to the others (> 500 nm) and thus relatively high specific surface area of 4.0 m^2 g^{-1}. On the other hand, SSR methods for both (one and two steps) procedures produced considerably large particles (> 500 nm) even at 973 K. Although elevating temperature in 2PC method causes appreciable crystal growth to some extent, the obtained particles are still much smaller. These findings indicate that the use of smaller

Bi_3TaO_7 particles prepared *via* PC methods is quite effective and essential for producing much smaller particles of Bi_4TaO_8Cl having higher specific surface area.

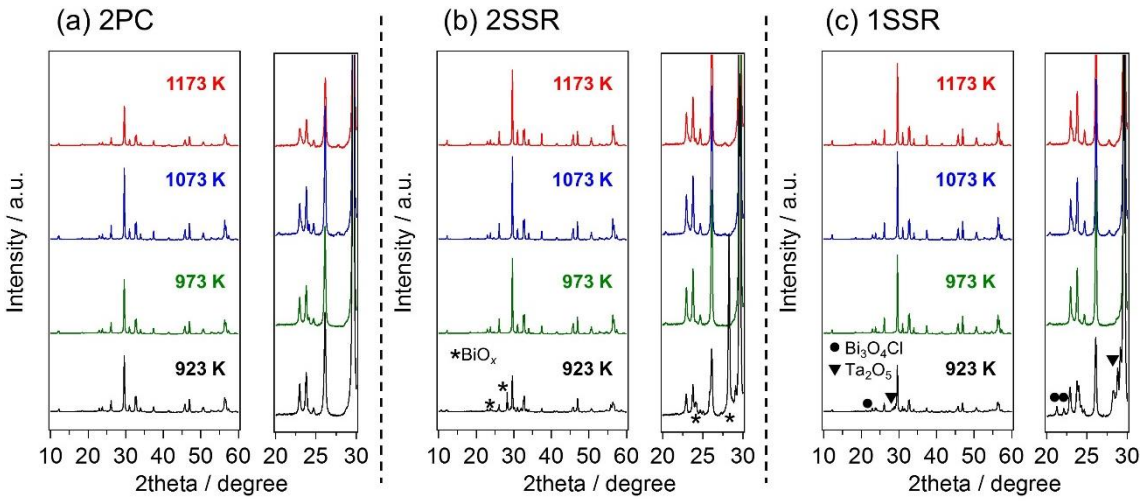

Fig. 1. XRD patterns of Bi_4TaO_8Cl samples prepared under various conditions. The right-hand small panels indicate enlarged patterns around impurities.

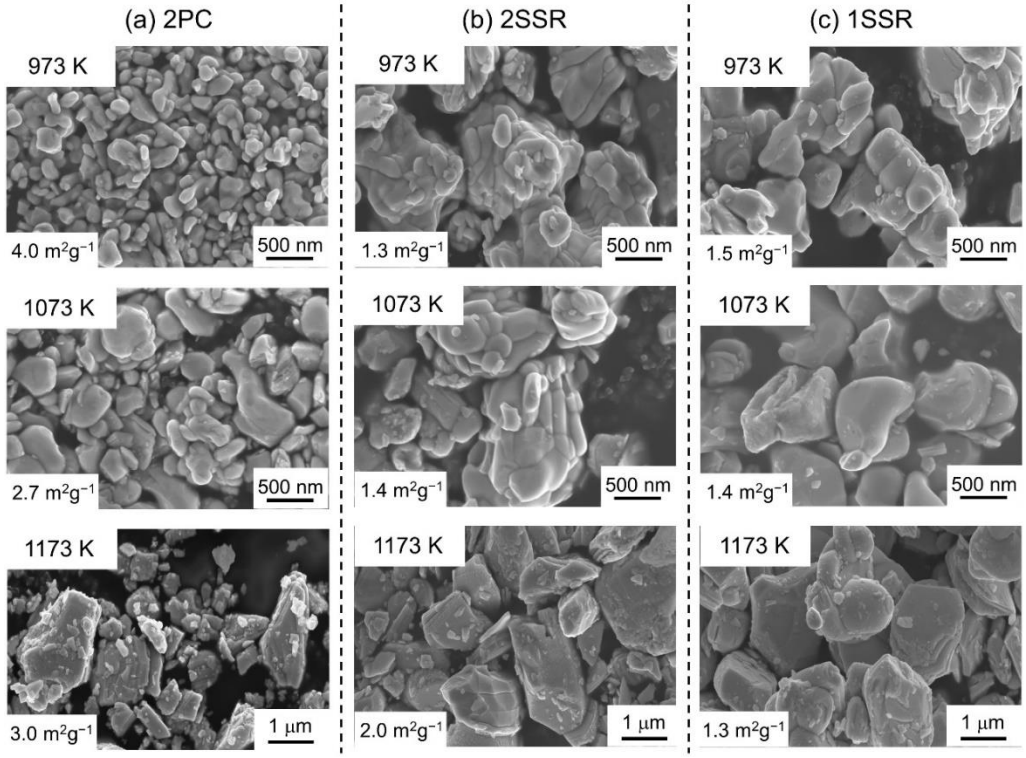

Fig. 2. SEM images of Bi_4TaO_8Cl samples prepared under various conditions.

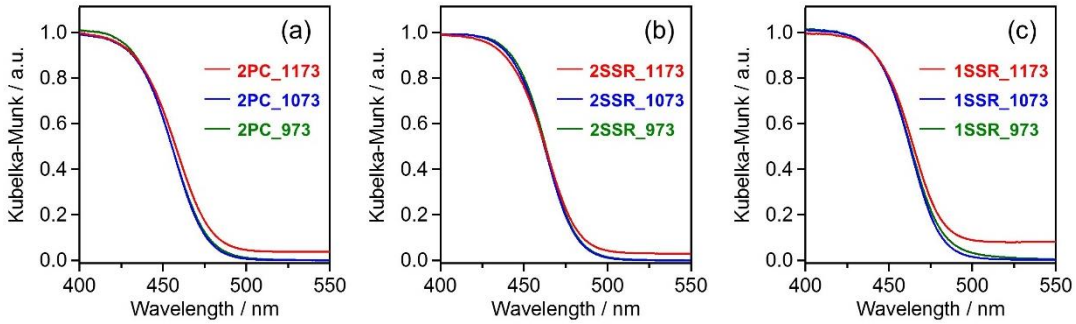

Fig. 3. DRS of Bi_4TaO_8Cl samples prepared under various conditions.

In all cases, the growth of crystals is observed with increasing calcination temperature. At the same time, however, very small crystals are also observed when calcined at 1173 K, particularly in 2PC_1173, whereas such small ones are hardly observed at lower temperatures (Fig. 2). We have observed similar phenomena in our recent study on the preparation of Bi_4MO_8X (*M*: Nb, Ta; *X*: Cl, Br) particles by the 1SSR method.[28] These small particles should be broken pieces of crystals during the high-temperature calcination. As a result, specific surface areas of the Bi_4TaO_8Cl samples prepared *via* 2PC and 2SSR obviously increased with increasing the calcination temperature from 1073 to 1173 K, in stark contrast to conventional oxide materials in which the increase in calcination temperature causes the decrease in specific surface area due to crystal growth. This unusual phenomenon observed in the present Bi_4TaO_8Cl samples can be explained by the volatile nature of chlorine species during high temperature calcination.

Fig. 3 compares UV-vis diffuse reflectance spectra of Bi_4TaO_8Cl samples prepared under various conditions. Although all the samples exhibited identical absorption edge at around 480 nm corresponding to the bandgap transition of 2.5 eV, one can notice a broad absorption at $\lambda \geq 480$ nm for the samples prepared at 1173 K, in particular, 1SSR_1173, which is often derived from the presence of anion defects and/or reduced species of cations.[36]

We conducted quantitative analysis of Cl^- composition by means of angle-resolved XPS (ARXPS) measurements. The ARXPS technique provides information of near surface with higher selectivity by decreasing the take-off angle between the plane of the surface and the analyser axis (generally 45 degrees is used in normal XPS). As summarized in Table 1, the Cl/Bi ratios determined by the normal XPS analysis (45 degree) slightly but certainly decreased from the stoichiometric ratio (0.25) upon increasing calcination temperatures, especially for the samples prepared at 1173 K, independent of the synthesis procedures (SSR/PC). The decrease in Cl/Bi becomes more evident when the take-off angle is reduced to 15 degrees. This observation strongly supports the generation of Cl^- defects at the outmost surface region, during calcination at high temperature. Our previous study on the synthesis of Bi_4MO_8X (*M*: Nb, Ta; *X*: Cl, Br) samples by 1SSR revealed that halogen defects can be generate by high temperature calcination due to the evaporation of halogens even when a sealed tube system is employed. In addition, the excess use of halogen precursor (*e.g.*, BiO*X*) was found to effectively suppress the formation of such halogen defects, resulting in higher photocatalytic activity for water oxidation in the presence of Ag^+ electron acceptor.[28] This is the reason why we synthesized all the Bi_4TaO_8Cl samples with a 5 mol% excess of BiOCl. However, the formation Cl^- defects could not be completely avoided at high temperature calcination, indicating the importance of low-temperature synthesis for the oxyhalide photocatalysts.

Table 1. Cl/Bi Atomic Ratios Estimated by Angle-Resolved XPS for Bi_4TaO_8Cl Samples Prepared under Various Conditions.

Sample	Cl/Bi (45 degree)	Cl/Bi (15 degree)
2PC_973	0.25	0.25
2PC_1073	0.24	0.22
2PC_1173	0.23	0.22
2SSR_973	0.25	0.24
2SSR_1073	0.25	0.23
2SSR_1173	0.23	0.21
1SSR_973	0.26	0.25
1SSR_1073	0.25	0.24
1SSR_1173	0.24	0.22

Photocatalytic water oxidation with an Fe^{3+} electron acceptor using Bi_4TaO_8Cl prepared at various conditions

Photocatalytic activities of the present Bi_4TaO_8Cl samples were evaluated by a half reaction of Z-scheme water splitting, *i.e.*, oxidation of water to O_2 accompanied by the reduction of Fe^{3+} to Fe^{2+}. Fig. 4 shows typical time courses of photocatalytic O_2

evolution from an aqueous $FeCl_3$ solution under visible-light irradiation ($\lambda > 400$ nm) over the three Bi_4TaO_8Cl samples that were synthesized *via* three different procedures (2PC vs. 1SSR vs. 2SSR) at a fixed calcination temperature of 973 K. The 2PC_973 sample showed much higher rate of O_2 evolution than the others, which likely reflects the high specific surface area of 2PC_973 (4.0 m^2g^{-1}), compared to 1SSR_973 (1.5 m^2g^{-1}) and 2SSR_973 (1.3 m^2g^{-1}). The rate of O_2 evolution on the 2PC_973 sample slightly decreases with prolonged time, due to the competing backward oxidation of Fe^{2+}, the concentration of which increased with proceeding photocatalytic water oxidation with reduction of Fe^{3+},[37] not to the deactivation of photocatalyst itself. The sufficient stability of the Bi_4TaO_8Cl samples prepared *via* 2PC was indeed proven by the results of overall Z-scheme water splitting, as shown in a later section. It should be noted here that the samples prepared by SSR methods (1SSR_973 and 2SSR_973) exhibited quite similar properties (*i.e.*, photocatalytic activity, specific surface area, and primary particle size). Thus, more detailed investigation of temperature dependence on the photocatalytic activity was carried out by using samples prepared *via* 2PC and 1SSR methods.

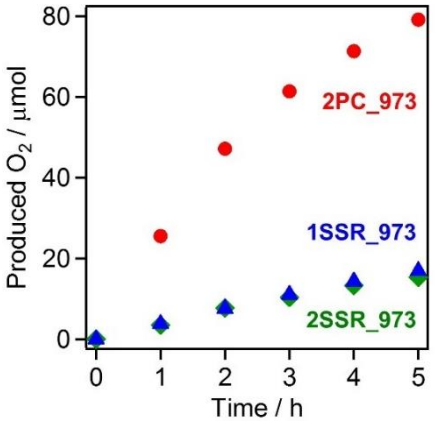

Fig. 4. Time courses of O_2 generation over Bi_4TaO_8Cl samples prepared under various procedure at 973 K in aqueous $FeCl_3$ solution (5 mM, pH = 2.5 adjusted by HCl) under visible-light irradiation ($\lambda > 400$ nm).

Fig. 5 summarizes the initial rate of O_2 evolution on Bi_4TaO_8Cl samples synthesized *via* 2PC and 1SSR methods at different calcination temperatures. Clearly, the Bi_4TaO_8Cl samples synthesized *via* 2PC exhibit higher rate than those *via* 1SSR at any calcination temperatures. This is reasonable given the higher specific surface areas for the former (see Fig. 2). The 2PC_973 sample exhibited the highest activity.

Interestingly, 1SSR and 2PC based samples showed quite different trend in activity in terms of calcination temperature dependence. In 1SSR, the rate of O_2 evolution increased with increasing temperature up to 1173 K and then drastically decreased at 1223 K. In contrast, the rate of O_2 evolution on 2PC samples increased from 923 to 973 K but decreased at higher temperatures. The preparation temperature affects important properties as the photocatalyst, *i.e.*, particle sizes associated with the surface area and the distance of charge transport from the bulk to surface,[38] and formation of crystal defects which frequently serves to accelerate charge recombination processes.[39]

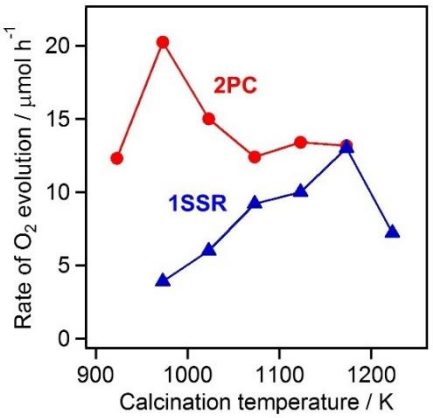

Fig. 5. Initial rates of O_2 evolution over Bi_4TaO_8Cl samples prepared under various conditions. Dispersion of Bi_4TaO_8Cl in aqueous $FeCl_3$ solution (5 mM, pH = 2.5 adjusted by HCl) was irradiated at $\lambda > 400$ nm.

To examine the charge dynamics in the present Bi_4TaO_8Cl, we employed time-resolved microwave conductivity (TRMC) measurements. TRMC has been reported as a powerful tool to provide an access to the local mobility and lifetimes of photogenerated charge carriers without electrode.[40] Fig. 6 shows transient photoconductivity assigned to photogenerated electrons, the main carriers in n-type Bi_4TaO_8Cl. The 1SSR_1173 sample exhibited longer lifetime τ obtained from a stretched exponential fitting (Fig. S3) of 0.23 μs than 1SSR_973 (τ = 0.08 μs), indicating less deactivation of electrons in 1SSR_1173 (Fig. 6a). Given the almost same particle sizes and surface areas for samples synthesized *via* 1SSR at 973 − 1173 K (see Fig. 2), the long-lived electrons, which is probably associated with the increased crystallinity (*i.e.*, decreased crystal defects), and account for the improved activity with increasing temperature up to 1173 K. The notable deactivation for the sample synthesized at 1223 K is probably caused by the increased surface defects (chloride and/or oxygen), along with the destruction of layers, as seen in the SEM images and surface Cl/Bi ratio (Fig. S4).

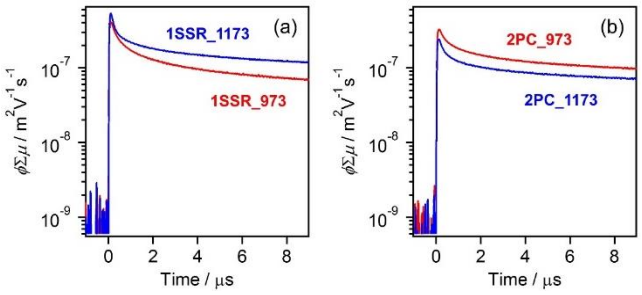

Fig. 6. Transient photoconductivities of samples excited by 355 nm laser.

Importantly, the 2PC_973 sample showing the most active photocatalytic performance exhibited long-lived electrons on the CB (τ = 0.42 μs) in comparison with 1SSR_973 (τ = 0.08 μs) (red curves in Figs. 6a and 6b), even compared with 1SSR_1173 (τ = 0.23 μs). It has been reported for some metal oxide

materials that the PC methods allow homogeneous (atomic level) mixing of precursors,[41] giving high-quality crystals, with sufficiently low concentration of charge recombination center such as anion defects.[34,42] Additionally, the 2PC_973 sample with smaller average particle size (Fig. 2) possesses significantly higher surface area. These two favourable properties would lead to the highest photocatalytic activity for water oxidation. Although the further elongation of τ (0.59 μs) was observed for 2PC_1173, its $\phi\Sigma\mu$ maximum (Fig. 6b) and specific surface area (Fig. 2) were decreased, which should be consistent with the drop in the rate of O_2 evolution (Fig. 5). The decreased activity for the samples annealed higher than 973 K also be linked to the decrease of surface area as seen in Fig. 2. In addition, high temperature treatment (> 1073 K) caused a partial crystal destruction and generation of Cl^- defects around outmost surface (see Fig. 2 and Table 1), possibly lowering the photocatalytic activity as well. On the other hand, the synthesis at 923 K might be insufficient for crystallization and induced lower photocatalytic activity than 2PC_973; the surface composition of Cl/Bi (0.24) was slightly low from stoichiometric ratio (Fig. S4), which was different from 2PC_973 (0.25).

Z-scheme water splitting using Bi_4TaO_8Cl as an O_2-evolving photocatalyst

Z-scheme water splitting under visible light was demonstrated by using the Bi_4TaO_8Cl samples as an O_2-evolving photocatalyst combined with Rh-doped $SrTiO_3$ (loaded with Ru cocatalyst)[43] as a H_2-evolving photocatalyst and an electron mediator of an Fe^{3+}/Fe^{2+} shuttle redox. As seen in Fig. 7, the use of 2PC_973 resulted in steady, simultaneous and stoichiometric generation of H_2 and O_2 with more than twice higher rates than the reaction with 1SSR_1173. Although such simultaneous generation also occurs even without Fe^{3+}/Fe^{2+} redox (Fig. S5) *via* direct electron transfer between two photocatalysts,[44] the rates (H_2: 3 μmol h^{-1}, O_2: 1.5 μmol h^{-1}) were much lower than those obtained by the use of Bi_4TaO_8Cl (2PC_973) sample with Fe^{3+}/Fe^{2+} redox. The photocatalytic reactions Bi_4TaO_8Cl alone (i.e., without $SrTiO_3$:Rh, shown in Fig. 4) did not gave any H_2 gas, indicating that the Bi_4TaO_8Cl worked as O_2-evolving photocatalyst rather than H_2-evolvong one under the present reaction conditions. On the other hand, it has been proven that the $SrTiO_3$:Rh photocatalyst has no ability of water oxidation.[45] These results strongly suggest that the majority of H_2 and O_2 was generated *via* electron transfer through redox cycle of Fe^{3+}/Fe^{2+} in the reaction with Bi_4TaO_8Cl (2PC_973) photocatalyst. Notably, $FeCl_3$ repeatedly mediated electron transfer *via* the Fe^{3+}/Fe^{2+} redox cycle because total amount of O_2 produced after 20-h irradiation (225 μmol) exceeded the stoichiometric amount (63 μmol), indicating that the Fe^{3+} added into the initial reaction solution was completely consumed according to eq. 2.

$$2H_2O + 4Fe^{3+} \rightarrow O_2 + 4Fe^{2+} + 4H^+ \quad (2)$$

The apparent quantum efficiency (AQY) for water splitting was determined to be 0.9% based on rates of H_2 and O_2 formation (1.8 and 0.9 μmol h^{-1}, respectively) on the combination of Bi_4TaO_8Cl (2PC_973) and Ru/$SrTiO_3$:Rh photocatalyst using 420-nm monochromatic light (2.2×10^{-7} einstein s^{-1}). The reaction under the same condition with Bi_4TaO_8Cl (1SSR_1173) sample resulted in lower quantum efficiency of 0.4%. The difference in the observed AQY well reflects the activity of each Bi_4TaO_8Cl sample for half reaction (*i.e.*, water oxidation with Fe^{3+} acceptor). These results clearly indicate the importance and effectiveness of improving the efficiency of O_2-evolving photocatalyst to improve the whole efficiency of Z-scheme water splitting. The rate of gas evolution through the Z-scheme water splitting using 2PC_973 as the O_2-evolution photocatalyst (11 μmol h^{-1} for O_2 evolution) was larger than that using Bi_4TaO_8Cl prepared by a flux method (2 μmol h^{-1}) with similar experimental setup,[46] although simple comparison is not available.

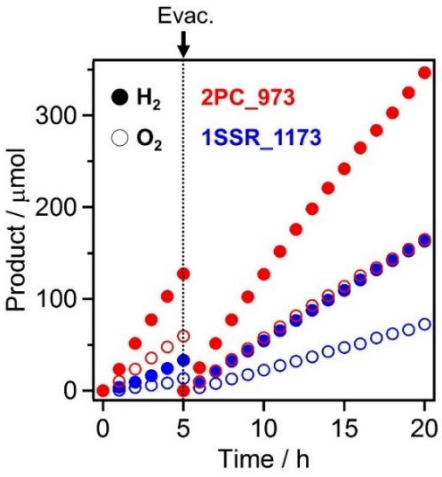

Fig. 7. Time courses of photocatalytic water splitting into H_2 and O_2 from a mixture of Bi_4TaO_8Cl (2PC_973) and Ru/$SrTiO_3$:Rh in aqueous $FeCl_3$ solution (1 mM, pH = 2.5 adjusted by HCl) under visible-light irradiation (λ > 400 nm).

Versatility of the two-step synthesis for other layered-oxyhalide materials

The results on Bi_4TaO_8Cl led us to apply the 2PC synthesis to other Sillén-Aurivillius and related layered-oxyhalide materials, for which only SSR synthesis has been reported.[26,27] As seen in Fig. S6, Bi_4NbO_8Cl and $Bi_6NbWO_{14}Cl$ could be prepared *via* similar 2PC synthesis involving Bi_3NbO_7 and Bi_5NbWO_{13} precursors. Importantly, the 2PC procedure enabled the synthesis of a new Sillén-Aurivillius oxychloride $Sr_2Bi_3Ta_2O_{11}Cl$ having a Ta-based double perovskite layer with much more mild calcination (*i.e.*, 1123 K for 15 h in 2PC and 1223 K for 35 h in 1SSR).

Fig. 8 shows results of Z-scheme water splitting using Bi_4NbO_8Cl, $Bi_6NbWO_{14}Cl$, or $Sr_2Bi_3Ta_2O_{11}Cl$ as the O_2-evolving photocatalyst coupled with Ru/$SrTiO_3$:Rh and the Fe^{3+}/Fe^{2+} redox mediator. The higher rates of gas evolution (H_2 and O_2) were attained for photocatalysts prepared by the 2PC method in compared to the corresponding samples papered by the 1SSR method. Especially, significant improvement of the photocatalytic activity was observed by using $Sr_2Bi_3Ta_2O_{11}Cl$. Since relatively harsh condition (1223 K for 35 h) was required in the 1SSR method to obtain pure $Sr_2Bi_3Ta_2O_{11}Cl$, excessive crystal growth was unavoidable as seen in Fig. 9. On the other hand, the 2PC method effectively eased the required conditions (1123 K for 15 h) to produce pure phase and therefore provided

highly active $Sr_2Bi_3Ta_2O_{11}Cl$ photocatalyst. Bi_4TaO_8Cl showed best photocatalytic performance among the oxyhalide materials employed in the present study although the origin is still unclear because of their different bandgaps and levels in addition to various physicochemical properties.

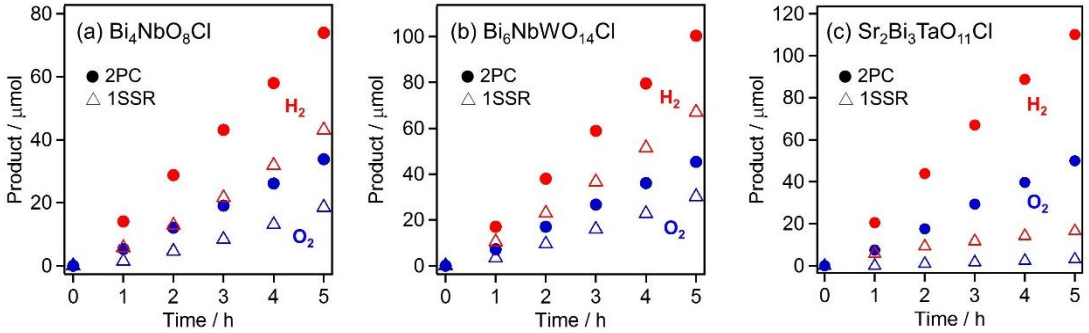

Fig. 8. Time courses of photocatalytic water splitting into H_2 and O_2 from (a) Bi_4NbO_8Cl, (b) $Bi_6NbWO_{14}Cl$, and (c) $Sr_2Bi_3Ta_2O_{11}Cl$ combined with $Ru/SrTiO_3$:Rh in aqueous $FeCl_3$ solution (1 mM, pH = 2.5 adjusted by HCl) under irradiation of visible light (λ > 400 nm for (a) and (b)) or UV-visible light (λ > 350 nm for (c)).

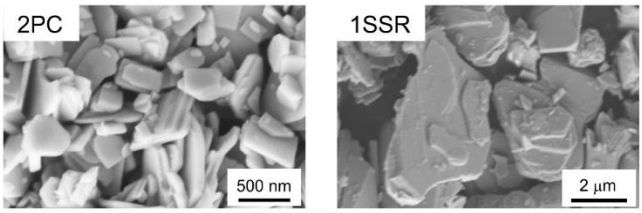

Fig. 9. SEM images of $Sr_2Bi_3Ta_2O_{11}Cl$ prepared by 2PC and 1SSR methods.

Conclusions

We developed a two-step synthesis of Sillén-Aurivillius and related layered oxyhalides, which successfully enhanced their photocatalytic activity for Z-scheme water splitting. For Bi_4TaO_8Cl, the best photocatalytic activity was recorded, with the apparent quantum efficiency (AQY) of 0.9% for Z-scheme water splitting in combination with $Ru/SrTiO_3$:Rh and a Fe^{3+}/Fe^{2+} redox mediator, which is more than two-fold higher than that prepared by a standard solid-state reaction (0.4%). Importantly, time-resolved microwave conductivity measurements revealed that 2PC-based sample exhibited long-lived charge separated states. The ordinal solid-state reaction required high temperature (1173 K) to accelerate charge separation although it accompanied decrease of surface areas and increase of surface Cl^- defects. Such negative aspects should be the essential problem in the synthesis of the oxyhalide materials by conventional solid-state reaction at high temperature. On the other hand, the use of nanopariculate Bi_3TaO_7 precursor *via* polymerized complex method enabled low temperature preparation (973 K) of the highly active Bi_4TaO_8Cl photocatalyst having both high specific surface area and less chlorine deficiency around the surface. We further demonstrated that this synthetic strategy is widely applicable to other layered perovskite oxyhalides including $Sr_2Bi_3Ta_2O_{11}Cl$ which is the first Sillén-Aurivillius photocatalyst having a Ta-based double perovskite slab and found to be effective for enhancement of their photocatalytic activities as well. The present work thus indicates that the suppressing deficiency of more volatile halide anion (vs. oxide anion) by low temperature preparation but maintaining bulk charge separation efficiency, along with downsizing of particles, is essential in improving photocatalytic activities.

Conflicts of interest

There are no conflicts to declare.

Acknowledgements

This work was supported by the CREST (JPMJCR1421), JSPS KAKENHI (JP17H06439, JP16H06439, JP16H06441, and JP15H03849), and Japan Society for the Promotion of Science (JSPS) Core-to-Core Program (A) Advanced Research Networks. The authors are also indebted to the technical division of Institute for Catalysis, Hokkaido University for their help in building the experimental equipment.

Notes and references

1 M. Tabata, K. Maeda, M. Higashi, D. Lu, T. Takata, R. Abe and K. Domen, *Langmuir*, 2010, **26**, 9161–9165.
2 K. Maeda, R. Abe and K. Domen, *J. Phys. Chem. C*, 2011, **115**, 3057–3064.
3 S. S. K. Ma, K. Maeda, T. Hisatomi, M. Tabata, A. Kudo and K. Domen, *Chem. – A Eur. J.*, 2013, **19**, 7480–7486.
4 A. Nakada, S. Nishioka, J. J. M. Vequizo, K. Muraoka, T. Kanazawa, A. Yamakata, S. Nozawa, H. Kumagai, S. Adachi, O. Ishitani and K. Maeda, *J. Mater. Chem. A*, 2017, **5**, 11710–11719.
5 Y. Iwase, O. Tomita, M. Higashi and R. Abe, *Sustain. Energy Fuels*, 2017, **1**, 748–754.
6 K. Maeda, Y. Shimodaira, B. Lee, K. Teramura, D. Lu, H. Kobayashi and K. Domen, *J. Phys. Chem. C*, 2007, **111**, 18264–18270.
7 K. Maeda, K. Teramura, D. Lu, T. Takata, N. Saito, Y. Inoue and K. Domen, *Nature*, 2006, **440**, 295.
8 S. Chen, Y. Qi, T. Hisatomi, Q. Ding, T. Asai, Z. Li, S. S. K. Ma, F. Zhang, K. Domen and C. Li, *Angew. Chemie Int. Ed.*, 2015, **54**, 8498–8501.
9 C. Pan, T. Takata and K. Domen, *Chem. - A Eur. J.*, 2016, **22**, 1854–1862.

10 A. Iwase, S. Yoshino, T. Takayama, Y. H. Ng, R. Amal and A. Kudo, *J. Am. Chem. Soc.*, 2016, **138**, 10260–10264.
11 T. Shirakawa, M. Higashi, O. Tomita and R. Abe, *Sustain. Energy Fuels*, 2017, **1**, 1065–1073.
12 W. Wang, J. Chen, C. Li and W. Tian, *Nat. Commun.*, 2014, **5**, 1–8.
13 S. Sun, T. Hisatomi, Q. Wang, S. Chen, G. Ma, J. Liu, S. Nandy, T. Minegishi, M. Katayama and K. Domen, *ACS Catal.*, 2018, **8**, 1690–1696.
14 G. Ma, S. Chen, Y. Kuang, S. Akiyama, T. Hisatomi, M. Nakabayashi, N. Shibata, M. Katayama, T. Minegishi and K. Domen, *J. Phys. Chem. Lett.*, 2016, **7**, 3892–3896.
15 K. Maeda, *Phys. Chem. Chem. Phys.*, 2013, **15**, 10537–10548.
16 H. Kageyama, K. Hayashi, K. Maeda, J. P. Attfield, Z. Hiroi, J. M. Rondinelli and K. R. Poeppelmeier, *Nat. Commun.*, 2018, **9**, 772.
17 M. Hara, G. Hitoki, T. Takata, J. N. Kondo, H. Kobayashi and K. Domen, *Catal. Today*, 2003, **78**, 555–560.
18 G. Hitoki, T. Takata, J. N. Kondo, M. Hara, H. Kobayashi and K. Domen, *Chem. Commun.*, 2002, 1698–1699.
19 M. Higashi, R. Abe, K. Teramura and T. Takata, *Chem. Phys. Lett.*, 2008, **452**, 120–123.
20 F. Zhang, A. Yamakata, K. Maeda, Y. Moriya, T. Takata, J. Kubota, K. Teshima, S. Oishi and K. Domen, *J. Am. Chem. Soc.*, 2012, **134**, 8348–8351.
21 B. Siritanaratkul, K. Maeda, T. Hisatomi and K. Domen, *ChemSusChem*, 2011, **4**, 74–78.
22 N. Buehler, K. Meier and J. F. Reber, *J. Phys. Chem.*, 1984, **88**, 3261–3268.
23 K. Maeda and K. Domen, *J. Catal.*, 2014, **310**, 67–74.
24 H. Kunioku, M. Higashi, O. Tomita, M. Yabuuchi, D. Kato, H. Fujito, H. Kageyama and R. Abe, *J. Mater. Chem. A*, 2018, **6**, 3100–3107.
25 D. Kato, K. Hongo, R. Maezono, M. Higashi, H. Kunioku, M. Yabuuchi, H. Suzuki, H. Okajima, C. Zhong, K. Nakano, R. Abe and H. Kageyama, *J. Am. Chem. Soc.*, 2017, **139**, 18725–18731.
26 H. Fujito, H. Kunioku, D. Kato, H. Suzuki, M. Higashi, H. Kageyama and R. Abe, *J. Am. Chem. Soc.*, 2016, **138**, 2082–2085.
27 H. kunioku, M. Higashi, C. Tassel, D. Kato, O. Tomita, H. Kageyama and R. Abe, *Chem. Lett.*, 2017, **46**, 583–586.
28 H. kunioku, A. Nakada, M. Higashi, O. Tomita, H. Kageyama, R. Abe, *Sustain. Energy Fuels,* in press. DOI: 10.1039/C8SE00097B.
29 A. Nakamura, O. Tomita, M. Higashi, S. Hosokawa, T. Tanaka and R. Abe, *Chem. Lett.*, 2015, **44**, 1001–1003.
30 K. Maeda, H. Terashima, K. Kase and K. Domen, *Appl. Catal. A Gen.*, 2009, **357**, 206–212.
31 K. Maeda, N. Nishimura and K. Domen, *Appl. Catal. A Gen.*, 2009, **370**, 88–92.
32 S. Nishioka and K. Maeda, *RSC Adv.*, 2015, **5**, 100123–100128.
33 A. Kudo, K. Omori and H. Kato, *J. Am. Chem. Soc.*, 1999, **121**, 11459–11467.
34 H. Kato, Y. Sasaki, N. Shirakura and A. Kudo, *J. Mater. Chem. A*, 2013, **1**, 12327–12333.
35 R. Konta, T. Ishii, H. Kato and A. Kudo, *J. Phys. Chem. B*, 2004, **108**, 8992–8995.
36 N. Murakami, O. O. P. Mahaney, R. Abe, T. Torimoto and B. Ohtani, *J. Phys. Chem. C*, 2007, **111**, 11927–11935.
37 H. Kato, Y. Sasaki, A. Iwase and A. Kudo, *Bull. Chem. Soc. Jpn.*, 2007, **80**, 2457–2464.
38 A. Kudo and Y. Miseki, *Chem. Soc. Rev.*, 2009, **38**, 253–278.
39 O.-O. Prieto-Mahaney, N. Murakami, R. Abe and B. Ohtani, *Chem. Lett.*, 2009, **38**, 238–239.
40 A. Saeki, S. Yoshikawa, M. Tsuji, Y. Koizumi, M. Ide, C. Vijayakumar and S. Seki, *J. Am. Chem. Soc.*, 2012, **134**, 19035–19042.
41 M. Kakihana, *J. Sol-Gel Sci. Technol.*, 1996, **6**, 7–55.
42 S. Ikeda, M. Hara, J. N. Kondo, K. Domen, H. Takahashi, T. Okubo and M. Kakihana, *Chem. Mater.*, 1998, **10**, 72–77.
43 Y. Sasaki, A. Iwase, H. Kato and A. Kudo, *J. Catal.*, 2008, **259**, 133–137.
44 Y. Sasaki, H. Nemoto, K. Saito and A. Kudo, *J. Phys. Chem. C*, 2009, **113**, 17536–17542.
45 R. Konta, T. Ishii, H. Kato, A. Kudo, *J. Phys. Chem. B*, 2004, **108**, 8992–8995.
46 X. Tao, Y. Zhao, L. Mu, S. Wang, R. Li, C. Li, *Adv. Energy Mater.* 2017, 1701392.

TOC

A two-step synthesis through polymerized-complex reaction remarkably improved photocatalytic activity of Sillén-Aurivillius type oxychlorides for Z-scheme water splitting.